



HAL
open science

Dual color localization microscopy of cellular nanostructures

Manuel Gunkel, Fabian Erdel, Karsten Rippe, Paul Lemmer, Rainer Kaufmann, Christoph Hörmann, Roman Amberger, Christoph Cremer

► **To cite this version:**

Manuel Gunkel, Fabian Erdel, Karsten Rippe, Paul Lemmer, Rainer Kaufmann, et al.. Dual color localization microscopy of cellular nanostructures. *Biotechnology Journal*, 2009, 4 (6), pp.927. 10.1002/biot.200900005 . hal-00494027

HAL Id: hal-00494027

<https://hal.science/hal-00494027>

Submitted on 22 Jun 2010

HAL is a multi-disciplinary open access archive for the deposit and dissemination of scientific research documents, whether they are published or not. The documents may come from teaching and research institutions in France or abroad, or from public or private research centers.

L'archive ouverte pluridisciplinaire **HAL**, est destinée au dépôt et à la diffusion de documents scientifiques de niveau recherche, publiés ou non, émanant des établissements d'enseignement et de recherche français ou étrangers, des laboratoires publics ou privés.



Dual color localization microscopy of cellular nanostructures

Journal:	<i>Biotechnology Journal</i>
Manuscript ID:	biot.200900005.R2
Wiley - Manuscript type:	Research Article
Date Submitted by the Author:	10-May-2009
Complete List of Authors:	Gunkel, Manuel; University Heidelberg, Kirchhoff-Institute for Physics Erdel, Fabian; Deutsches Krebsforschungszentrum, Research Group Genome Organization and Function Rippe, Karsten; Deutsches Krebsforschungszentrum, Research Group Genome Organization and Function Lemmer, Paul; University Heidelberg, Kirchhoff-Institute for Physics Kaufmann, Rainer; University Heidelberg, Kirchhoff-Institute for Physics Hörmann, Christoph; University Heidelberg, Kirchhoff-Institute for Physics Amberger, Roman; University Heidelberg, Kirchhoff-Institute for Physics Cremer, Christoph; University Heidelberg, Kirchhoff-Institute for Physics
Keywords:	SPDM, localization microscopy, molecular imaging, nanobiophotonics, 2CLM



Research Article ((6366 words))**Dual color localization microscopy of cellular nanostructures**

Manuel Gunkel¹, Fabian Erdel², Karsten Rippe², Paul Lemmer¹, Rainer Kaufmann¹,
Christoph Hörmann¹, Roman Amberger¹, Christoph Cremer^{1,3,4*}

¹ Kirchhoff-Institute for Physics & BioQuant Center University of Heidelberg, Im
Neuenheimer Feld 227, D-69120 Heidelberg, Germany

² Deutsches Krebsforschungszentrum & BioQuant Center University of
Heidelberg, Research Group Genome Organization & Function, Im Neuenheimer Feld 280,
D-69120 Heidelberg, Germany

³ Institute for Pharmacy and Molecular Biotechnology, University of Heidelberg, Im
Neuenheimer Feld 364, D-69120 Heidelberg, Germany

⁴ Institute for Molecular Biophysics, The Jackson Laboratory, 600 Main Street, Bar Harbor,
ME 04609, USA

*corresponding author: cremer@kip.uni-heidelberg.de

Deleted: Changes April 27 in

Yellow

Changes May 09 in red

Revised Version

09. May 09

Formatted: Left

ABSTRACT

The Dual Color Localization Microscopy (2CLM) presented here is based on the principles of Spectral Precision Distance Microscopy (SPDM) with conventional fluorochromes under special physical conditions. This technique allows us to measure the spatial distribution of single fluorescently labeled molecules in entire cells with an effective optical resolution comparable to macromolecular dimensions. Here, we describe the application of the 2CLM approach to the simultaneous nanoimaging of cellular structures using two fluorochrome types distinguished by different fluorescence emission wavelengths. The capabilities of 2CLM for studying the spatial organization of the genome in the mammalian cell nucleus are demonstrated for the relative distributions of two chromosomal proteins labeled with autofluorescent GFP and mRFP1 domains. The 2CLM images revealed quantitative information on their spatial relationships down to length-scales of 30 nm.

Keywords: 2CLM, SPDM, localization microscopy, molecular imaging, nanobiophotonics, superresolution fluorescence microscopy, chromatin, spectrally assigned localization microscopy (SALM)

1. INTRODUCTION

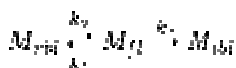
About 170 years ago, light microscopy facilitated the discovery of the cell as the fundamental unit of life, thus initiating one of the great revolutions of human science (for review see [1]). In the development of modern cell biology and its biomedical applications, however, analysis methods using visible light microscopy approaches often played a secondary role compared with biochemical techniques. A major reason for this was the optical resolution thought to be restricted to a fundamental limit of a few hundreds of nm laterally (and about 600 nm axially). Consequently, the nanostructure of cellular machines (e.g. the protein complexes responsible for molecular transport, DNA replication, transcription and repair, RNA splicing, protein synthesis and degradation), was not accessible to light microscopy. The same is true for the spatial organization of specific chromatin domains with a size in the hundred nm range that play an essential role for gene regulation [2]. As described in the famous publication of Ernst Abbe (1873) [3], this limit in light-optical resolution of about 200 nm was thought to be due to the wave nature of light ; it was regarded to be insurmountable according to the fundamental laws of physics. A very similar conclusion was obtained in 1896 by Lord Rayleigh [4]. However, a variety of laser-optical far field microscopy techniques based on fluorescence excitation has been developed recently to circumvent the Abbe/Rayleigh-limit of 200 nm. These make light-optical analysis of biological macromolecules by enhanced resolution possible. Some well known methods are 4Pi-Microscopy [5-6], structured/patterned illumination microscopy [7,8], STED microscopy [9,10] and spectrally assigned localization microscopy (SALM) approaches using far field fluorescence microscopy [11-28, 49 - 52]. With these techniques, an effective optical resolution in the 10 – 20 nm regime has been obtained. While STED microscopy is a focused beam method that allows it to rapidly image small regions of

interest (few μm extension), the complementary localization microscopy techniques are preferentially used in a non-focusing setup for rapidly imaging large regions of interest (50 – 100 μm extension).

The basis of SALM as a far field fluorescence microscopy approach is the independent localization of “point-like” objects excited to fluorescence emission by either focused or non-focused illumination techniques, typically with a laser. This means the localization is achieved by appropriate features of the fluorochromes resulting in an “optical isolation”. We refer to this approach as “Spectral Precision Distance (Position Determination) Microscopy” (SPDM). SPDM was already conceived and realized in proof-of-principle experiments in the 1990s [11 – 16,19]. Compared with related concepts [29 - 31], the SPDM approach relies on specific spectral signatures including all kinds of fluorescent emission parameters suitable, from absorption/emission spectra to fluorescence life times [13] to luminescence in general.

In the last few years, SALM methods have been improved considerably by several groups by making use of photoswitchable fluorochromes. In these approaches, fluorochromes are switched between a ‘dark’ state A and a ‘bright’ state B using a first laser wavelength λ_1 for switching from A to B and a second laser wavelength λ_2 from B to A. In this way, the position of the molecules was determined with precision values significantly better than the full width at half maximum (FWHM). These microscopic techniques were termed photoactivated localization microscopy (PALM) [20], fluorescence photoactivation localization microscopy (FPALM) [21], stochastic optical reconstruction microscopy (STORM) [22], PALM with independently running acquisition (PALMIRA) [23, 24], or “direct” STORM (dSTORM) [27]. In all these approaches, special fluorochromes were used which can be photoswitched between a “dark” state A and a “bright” state B [6].

Recently, we applied SPDM on the nanometer resolution scale to conventional fluorochromes. In contrast to the photoswitching based SALM methods cited above, one laser wavelength only is used to induce fluorescence/luminescence lifetimes in a given fluorochrome on the second time scale. In this case under special physical conditions “reversible photobleaching” [25, 26, 28] occurs. “Reversible photobleaching” has been shown to be a general behavior in several fluorescent proteins, e.g. GFP derivatives like CFP, GFP, Citrine or eYFP [34 - 36]. Under such conditions, the fluorescence emission of certain types can be described by assuming three different states of the molecule: A fluorescent state M_{fl} , a long living reversibly bleached state M_{rbl} , and an irreversibly bleached state M_{ibl} . Once the molecule returns from the M_{rbl} state to the M_{fl} state, it can be excited a large number of times (fluorescence bursts) until it passes into the irreversibly bleached state M_{ibl} (i.e. a dark state of a lifetime which is long compared with the acquisition time [34, 37]); and thus its position can be determined **with nanometer precision**



[25,26, 28]. With transition time constants k_1 , k_2 , k_3 one can assume the transition scheme [34]. We recently showed that reversible photobleaching can be used for superresolution imaging of cellular nanostructures labeled with conventional fluorochromes such as Alexa

1
2 488 [25, 37] or the Green Fluorescent Protein variant YFP [26]. This novel extension of the
3 SPDM approach to ordinary fluorophores was based on the possibility to produce the
4 optical isolation required by allowing only one molecule in a given observation volume and
5 in a given time interval to be in the M_{II} state. Such conditions were achieved by using an
6 excitation intensity in the 10 kW/cm^2 to 1 MW/cm^2 range. These conditions were equivalent
7 to switching the majority of the fluorophores to a metastable dark state and allowing the
8 spontaneous return to lower energy levels under the emission of fluorescence photons [49].
9 Recently, Foelling et al. [49] have described a related approach to obtain highly resolved
10 dual-color images of immunostained microtubules and peroxysomes using Atto 532 and
11 565 dyes. Here we present first results to extend the SPDM method to the localization of
12 two different molecule types in human cell nuclei ("Two color localization microscopy",
13 2CLM). Two types of nuclear proteins tagged with two different standard fluorescent
14 proteins were distinguished by different fluorescence emission wavelengths. 2CLM was
15 applied to "nanoimage" the spatial distribution of these proteins at molecular optical
16 resolution.

17 The organization of the DNA genome by proteins is a particular interesting subject for
18 2CLM microscopy studies. In the cell nucleus the DNA is compacted by histone proteins
19 into a nucleoprotein complex termed chromatin [38]. The central building block of chromatin
20 is the cylindrically shaped nucleosome (11 nm diameter, 5.5 nm height). It comprises an
21 octamer core of two copies each of histones H2A, H2B, H3 and H4 around which the DNA
22 is wrapped in 1.67 turns. In the present study the technique of 2CLM microscopy was used
23 to determine the intracellular location of chromatin remodeling complexes with respect to
24 chromatin. Chromatin remodelers are molecular machines that can translocate
25 nucleosomes along the DNA sequence upon hydrolysis of ATP [39 – 42]. By making use of
26 autofluorescent constructs of histone H2A as a nucleosome/chromatin marker and the
27 ATPase subunit Snf2H [41 – 43] that defines a certain class of chromatin remodeling
28 complexes, their nuclear localization was analyzed with an estimated mean localization
29 accuracy in the range of about 20 nm (ca. $1/25$ of the excitation wavelength). The results
30 indicate the feasibility to reveal details on the interaction of remodeling complexes with
31 chromatin at unprecedented effective resolution.

32 33 2. MATERIAL AND METHODS

34 35 2.1 Specimen preparation

36 Human U2OS osteosarcoma cells were cultured on 12-mm diameter glass coverslips in
37 Dulbecco's Modified Eagle medium supplemented with 10 % FCS for 1 day after plating.
38 Cells were transiently transfected with plasmid vectors for Snf2H-GFP and H2A-mRFP1
39 using Effectene (Qiagen) according to standard protocols. After transfection, cells were
40 cultured for 1 day, fixed in 4 % paraformaldehyde and then embedded with Mowiol 4-88
41 (Roth) as mounting medium. The plasmid pEGFP-N3-Snf2H was kindly provided by Patrick
42 Varga-Weisz and contains the full coding sequence of human Snf2H fused to GFP at the
43 C-terminus [43]. The plasmid pRSET-H2A-mRFP1 contains the full coding sequence of
44
45
46
47
48
49
50
51
52
53
54
55
56
57
58
59
60

1
2 human H2A with the red fluorescent mRFP1 domain at the C-terminus [Jegou, T. (2007)
3 PhD Thesis, University Heidelberg].
4

5 **2.2 Microscope setup**

6 In Fig. 1 the principal setup is shown schematically.
7

8 Due to the "bright" initial state (M_{II}) of the fluorochromes, specimens can be imaged in a
9 standard far-field conventional epifluorescence mode as well as in the 2CLM mode. The
10 specimens were illuminated by an Ar⁺-laser at $\lambda_{exc} = 488$ nm (excitation of GFP) or a Kr⁺-
11 laser at $\lambda_{exc} = 568$ nm (excitation of mRFP1), which were focused by the lens system L1 -
12 L3 and an objective lens 100x/NA1.4, oil (Leica, 35578 Wetzlar, Germany). This focusing
13 was modified in such a way that fluorescent molecules in the observation volume were
14 exposed to illumination intensities in the order of 50 – 200 kW/cm² within a broad region of
15 interest. The degree of focusing and thus the laser power density was adjusted by varying
16 the distances within the lens system along the optical axis. Under these conditions, suitable
17 fluorochromes as GFP and mRFP1 exhibited their characteristic reversible photobleaching
18 or light induced blinking, which was used to identify and spatially assign the localization of
19 individual molecules. Up to 70000 single molecules were detected in a region of interest of
20 about 20 $\mu\text{m} \times 20 \mu\text{m}$. Using a sensitive CCD camera (PCO, 93309 Kehlheim, Germany)
21 with a quadratic pixel size of 6.45 $\mu\text{m} \times 6.45 \mu\text{m}$ (1376 x 1040 pixels total) with a quantum
22 efficiency of up to 65 % for image acquisition, time series of 2D – images were acquired
23 with a repetition rate between 10 - 16 Hz. A typical time stack of 1500 images was typically
24 acquired within approximately 2 min. For further details, see [28].

25 An estimation of the chromatic shift was obtained by imaging fluorescently labeled 100 nm
26 beads under the same conditions used for the acquisition of 2CLM images. The positions
27 were determined in both channels and compared to each other. The mean chromatic shift
28 was found to be 5.6 ± 2.3 nm (see supplementary methods).
29

30 **2.3 Software for data registration and evaluation**

31 The microscopy data recorded were stored on a computer hard disk and evaluated later by
32 algorithms implemented in MATLAB (7.0.1, The MathWorks, Natick, USA), a matrix based
33 programming language for numerical computations. The algorithms were designed to
34 handle the data with high background noise and large variation of background due to
35 bleaching of the fluorochromes (e.g. dense labeling, large observation/activation volume)
36 as well as for a low noise scenario with negligible bleaching (e.g. photoactivatable
37 molecules in PALM/FPALM and/or small excitation volumes). The algorithm calculates the
38 following quantities [26, 28]:

- 39 • The position of the fluorescence signal in the object plane/in the object space
- 40 • Estimates for the localization accuracy (parameter errors are the diagonal elements
41 of the covariance matrix at convergence) on the single molecule level
- 42 • The characteristic parameters of the model function used to determine single
43 molecule positions
44

- Estimates for the number of detected photons per molecule as a decisive parameter of localization microscopy
- The position of the detected signal (individual molecule) in the data stack (i.e. image frame number) to analyze the influence of time and to extract relevant characteristics of the fluorochromes used

Following signal detection and registration, in a second step an optional preprocessing was performed. While signals with high signal-to-noise ratio (low background) can be used as raw data for the following data segmentation, in case of high background and photobleaching effects active during several succeeding image frames, an additional computing step was performed to segment signals originating from single molecules only. For this a differential photon stack $D_{Ph}(x, y, t') = S_{Ph}(x, y, t_{k+1}) - S_{Ph}(x, y, t_k)$ between two successive image frames (registered at t_k and t_{k+1}) was calculated. The error σ in photon number produced by the Poisson statistics of the incident photons and the noise σ_{CCD} of the CCD sensor detection (approx. 4 counts per pixel) was estimated by the Gaussian law

$$\sigma[D_{Ph}(x, y, t')] = \sqrt{(S_{Ph}(x, y, t_{k+1}))^2 + (S_{Ph}(x, y, t_k))^2 + 2\sigma_{CCD}^2}$$

of error propagation,

The data stacks $S_{Ph}(x, y, t)$ (in case of low background) and $D_{Ph}(x, y, t')$ (in case of high background) were then used for high precision localization of single molecules (lateral) by adapting modified Gaussian model functions. To reduce the computing efforts, Regions of Interest (ROIs) of typically 8x8 pixels were used, containing the signal.

Then a two dimensional Gaussian with a background gradient

$$f(x, y) = p_1 \exp\left[-\frac{(x - p_2)^2 + (y - p_3)^2}{p_4}\right] + p_5 + p_6(x - p_2) + p_7(y - p_3)$$

was fitted to the thresholded signals.

An appropriate set of values $p_1 - p_7$ was used as start parameters which were then optimized by the application of a Levenberg-Marquardt algorithm.

The final results were analyzed for parameter plausibility by additional filters. In this way molecules were localized in an observation volume with a thickness corresponding to an 'optical section' of 600 nm. For further details see [28].

3. RESULTS

3.1 The label density is critical for 2CLM experiments

1
2 To test the effects of the localization accuracy and the density of fluorescent molecules on
3 the appearance of the “nanoimages” obtained by 2CLM, the evaluation algorithms
4 described above were applied to simulated data. As an example, results obtained from a
5 simulated structure are presented. For this, the letters “2CLM” were scaled to an overall
6 length of 2 μm and a height of 0.4 μm (first row in Fig. 2). These four letters were then
7 simulated to contain single molecules with various densities (50000, 5000 and 500/ μm^2)
8 with a “fluorescence burst” emission. From these original images, conventional
9 epifluorescence images and 2CLM images were calculated as described elsewhere [28].

10 The result is presented in the second row of Fig. 2. The diffraction-limited widefield image
11 shows some alterations in the intensity distribution and gives an estimate of the overall size
12 of the “nanostructure”. A reconstruction of the original object, however, is clearly not
13 possible by assuming a “conventional” resolution (calculated PSF using numerical aperture
14 of 1.4, 100 nm effective pixel size of the detector and 520 nm (560 nm red letters) as
15 emission wavelength).

16 In the third row of Fig. 2 the image is shown for the application of the 2CLM approach
17 assuming a mean localization accuracy of 20 nm; a comparison with the original
18 “nanostructure” demonstrates the substantial resolution improvement. The third row shows
19 the simulation results for a localization accuracy of 10 nm. At a high (50000/ μm^2) or
20 medium (500/ μm^2) molecule density, the original “2CLM nano-object” can be fully
21 reconstructed. At a “low” molecule density, basic structural features can still be identified.
22 To summarize, the simulations show a) that the 2CLM method indeed allows us to extract
23 structural information far below the conventional resolution limit of epifluorescence
24 microscopy, b) that the density of molecules is a critical parameter, depending on the
25 structure to be studied.

26 27 28 **3.2 Nuclear distributions of H2A and Snf2H could be determined by 2CLM**

29 The lateral distribution of mRFP1 labeled H2A and GFP labeled Snf2H proteins in human
30 U2OS nuclei was determined by 2CLM within “optical sections” of about 600 nm thickness
31 in about 20 cells. These sections result from the fact, that the PSF of objects outside of the
32 focal plane is broadened up and thus has a worse signal-to-noise ratio (S/N). Accordingly,
33 these signals were filtered out by the fitting algorithm. In the mean, around 1,200 - 1, 800
34 photons per molecule were detected.

35 Figure 3 shows the distribution of mRFP1 labeled H2A proteins in a human U2OS nucleus
36 (size 12 μm x 18 μm). A conventional epifluorescence image was experimentally recorded
37 prior to the 2CLM measurement (Fig. 3A). The nucleoli can be clearly identified due to the
38 lower content of H2A histone proteins. Due to the limited optical resolution no further details
39 of the H2A distribution are apparent. The 2CLM data of the same nucleus are shown in Fig.
40 3B. A data stack consisting of 6000 individual images was recorded in four steps (1500
41 images acquired in each step due to the size of the PC memory) with a frame rate of about
42 16 Hz. Mechanical drift of the sample was corrected by correlating the summed signal of
43 each of those four stacks with the first one. The drift within one data stack was estimated to
44 be 12 nm (see supplementary material).

Deleted: ¶
¶
¶

1
2 In every image the positions of the blinking mRFP1 molecules were determined as
3 described in 2.3. The result is displayed in Fig. 3B: All 71156 registered positions of
4 individual H2A-mRFP1 signals are plotted together and blurred with a Gaussian according
5 to their localization accuracy. The mean localization accuracy was $\sigma = 38$ nm (see Fig. 6).
6

7 Figure 4 shows the distribution of GFP labeled Snf2H proteins in the same nucleus as
8 above. Again a conventional epifluorescence image (Fig. 4A) was acquired before 2CLM
9 imaging. Nucleoli cannot be identified in the epifluorescence nor the 2CLM image (Fig. 4).
10 In total 4500 images were recorded in three stacks. From these, 47062 positions of Snf2H
11 were determined with a mean localization accuracy of $\sigma = 26$ nm (see also Fig. 6).
12

13 In Fig. 5 the signal of both distributions is shown in the appropriate colors for comparison.
14 The same structures are visible in the epifluorescence (Fig. 5A) and the 2CLM image (Fig.
15 5B). Autofluorescence from unlabeled structures is not present in the 2CLM image.
16

17 3.3 Distribution analysis revealed partial colocalization between H2A and Snf2H

18 To characterize the nuclear distributions of H2A and Snf2H, the number of neighbors of the
19 same protein type within a 300 nm radius around each detected particle was determined in
20 a typical cell and plotted into a histogram (Fig. 7A,B). As a reference, the same histogram
21 was generated for random distributions with the corresponding particle densities. The
22 histograms for the random distributions could be fitted with a single Gaussian, whereas the
23 observed histograms for H2A and Snf2H were broader and had to be fitted with the sum of
24 two or three Gaussians. This reflects the heterogeneity in the H2A and Snf2H density and
25 the presence of low- and high-density populations for both H2A and Snf2H. To identify
26 these regions of different particle density, different colors were assigned (Fig. 7C,D). The
27 cut-off values were chosen to be the values at the intercept of the Gaussians used for fitting
28 the corresponding histogram. In order to detect also locations with the highest protein
29 density, the 10 % of the particles with the largest number of neighbors were depicted in
30 yellow. In the case of H2A, the sparse regions contained the nucleoli as expected.
31 However, additional regions which did not coincide with these nuclear compartments
32 appeared to be H2A-poor. The high-density regions of H2A (labeled green/yellow in Fig.
33 7C), which comprised about 55 % of the area of the cell nucleus, formed interconnected
34 patches including mostly regions located in the centre of the nucleus. In the case of Snf2H,
35 the sparse regions were found at the nuclear periphery. In the remaining part of the nucleus
36 Snf2H was distributed more homogeneously than H2A. In contrast to the H2A distribution,
37 the high-density regions of Snf2H (labeled green/yellow in Fig. 7D) comprised 36 % of the
38 area of the cell nucleus. In average, Snf2H molecules had 37 ± 12 neighbors, H2A
39 molecules had 52 ± 23 neighbors (intervals include 68 % of the molecules). Snf2H-rich
40 regions were located near the centre of the nucleus and often but not always corresponded
41 to H2A-rich regions (see arrows).
42

43 To analyze the colocalization of H2A and Snf2H, a correlation coefficient according to
44 Pearson of $R = 0.25$ was calculated for the images from Fig. 5 while $R = 0.13 - 0.17$ was
45 obtained for the random distributions. A value of 1 would represent perfect colocalization, a
46 value of -1 would represent perfect anti-colocalization. These results suggest a partial
47
48
49
50
51
52
53
54
55
56
57
58
59
60

1
2 colocalization between H2A and Snf2H that is compatible with transient interaction
3 behavior of the two proteins detected in FRAP experiments (data not shown). Similar
4 results were obtained by the analysis of the number of Snf2H molecules around H2A in a
5 typical cell and vice versa (Fig. 8). The average number of Snf2H molecules in the vicinity
6 of H2A (50 molecules within 300 nm radius) was significantly larger than the average
7 number of randomly distributed particles in the same region (41 molecules within 300 nm
8 radius) as confirmed by a Kolmogorov-Smirnov test (see supplementary material); the
9 same was true for H2A molecules in the vicinity of Snf2H (33 H2A molecules vs. 27
10 randomly distributed molecules within 300 nm radius). Further analysis of the histograms in
11 Fig. 8 was indicative of the presence of two particle populations, one with a large number of
12 neighbors and one with a small number of neighbors. Thus, the relative amounts of H2A
13 and Snf2H differ throughout the cell, suggesting the presence of chromatin regions with
14 locally enriched Snf2H concentration.

15 16 4. DISCUSSION

17 For the better understanding of functional cellular nanostructures, there is an urgent need
18 to circumvent the limitations of conventional light microscopy given by the Abbe/Rayleigh
19 limit of optical resolution. Multiple approaches for light optical analysis of biostructures at
20 enhanced resolution exist, with each of these having specific biological, biophysical and
21 biomedical applications. Recently, various methods of spectrally assigned localization
22 microscopy (SALM) have been shown to allow the nanoimaging of individual molecules at
23 an optical resolution close to the dimensions of small proteins.

24
25 In this report, SPDM with conventional fluorochromes under special physical conditions
26 was used to realize two color localization microscopy (2CLM). For each fluorochrome, only
27 one wavelength was sufficient for 2CLM. In this manner, the spatial distribution of two
28 different molecule types with distinct fluorescence emission wavelengths was obtained.

29 Under the conditions used (sampling time per image 60 – 100 ms) the percentage of
30 molecules appearing multiple times was estimated to be rather low. In previous publications
31 registered under at least the same mechanical stability and registration/evaluation
32 conditions [28], single molecule positions of fluorescent proteins can be distinguished
33 outside the nucleus, i.e. at very low molecule densities. A major percentage of multiple
34 appearance would have resulted in multiple small clusters. This was not observed.
35 Furthermore, in the 2CLM images presented here, a major percentage of multiple
36 appearance should be reflected in a strongly increased frequency of next neighbor
37 distances (Fig. 8) which also was not observed.

38 Since biological specimens labeled with such fluorescent proteins are most common, 2CLM
39 methods using such fluorochromes have a wide range of applications, including the
40 potential for in vivo measurements in cell cultures. In particular, they offer unique
41 possibilities for the functional characterization of molecular interactions between protein
42 complexes. This is demonstrated in the present work for the determination of the spatial
43 distribution of the Snf2H chromatin remodeler with respect to histone H2A as a
44 nucleosome/chromatin marker. Although chromatin remodeling complexes have been
45 shown in several studies to possess distinct nucleosome/DNA binding and remodeling
46
47
48
49
50
51
52
53
54
55
56
57
58
59
60

Deleted: ¶

¶
¶
¶

Deleted: ¶

1 capabilities in vitro (e.g. [39 – 42] and references therein), little is known on how they
2 operate in the cell. In a previous pioneering study Varga-Weisz and colleagues used
3 conventional confocal fluorescence microscopy at a lateral resolution of several 100 nm to
4 study Snf2H and its associated Acf1 subunit [43]. Their work revealed the overall
5 Snf2H/Acf1 nuclear distribution with an enrichment in pericentric heterochromatin foci
6 present in mouse cells, which have typical diameters of ~1 μm . 2CLM allowed an effective
7 optical resolution that was better by an order of magnitude so that the light microscopic
8 investigation of the interaction of Snf2H and other chromosomal proteins on the level of a
9 single nucleosome becomes feasible. We show how density maps with high resolution for
10 two different proteins in the same specimen can be generated and used to derive
11 information about the interaction behavior on different length scales (Fig. 8). On these
12 images, regions of increased nucleosome density can be identified from the H2A-mRFP1
13 signal, which could represent higher order structures of the folded nucleosome chain. The
14 Snf2H remodeler is distributed more homogeneously suggesting that a significant fraction
15 of Snf2H is not associated permanently with chromatin consistent with fluorescence
16 recovery after photobleaching experiments (Erdel & Rippe, private communication). While
17 the nuclear periphery was partially depleted from Snf2H virtually all other nuclear regions,
18 including the nucleolus, were accessible to the chromatin remodeler.
19

20 In Figure 7 several distinct regions with locally increased or decreased Snf2H density with
21 respect to H2A density are present that reflect a spatially altered interaction behavior
22 between Snf2H and H2A. In particular, several high-density Snf2H regions can be identified
23 that do not coincide with a strong H2A signal. Since it is expected that this increased Snf2H
24 density is connected with higher remodeling activity, these regions represent bona fide
25 chromatin remodeling hot spots that are likely to be loci of a pronounced translocation of
26 nucleosomes by Snf2H-containing molecular machines. Furthermore, sites of colocalization
27 of H2A and Snf2H are clearly present as inferred from the quantitative analysis (Fig. 8).
28 The closely co-localizing signals of single Snf2H-GFP and H2A-mRFP1 proteins may be
29 interpreted as complexes of Snf2H at a nucleosome. Thus, complexes of the chromatin
30 remodeler with its substrate can be detected by 2CLM. Compared with Fluorescence
31 Resonance Energy Transfer (FRET) methods, in addition to neighborhood estimates the
32 2CLM images allow such vicinity determinations of single complexes at distances not
33 accessible to FRET procedures. Additionally, 2CLM methods provide “true optical
34 resolution” in the region of about ten times better than conventional fluorescence
35 microscopy techniques and thus give also the spatial position of such complexes even in a
36 “crowded” nucleus. We anticipate that further studies along these lines in combination with
37 quantitative image analysis will provide valuable information on the molecular details of
38 nucleosome translocations by chromatin remodelers. Furthermore, the 2CLM investigations
39 of other chromosomal proteins associated with the genome will serve to derive spatial
40 molecular interaction maps for their organization in the nucleus.

41 | At an effective optical resolution down to the 10 - 20 nm range laterally in an optical section
42 of about 600 nm thickness, numerous other applications in the structural elucidation of
43 cellular nanostructures are feasible. Examples for such nanostructures are individual gene
44 domains in genetically active and inactive states [2], environmentally induced changes of
45

Deleted: ¶

1
2 chromatin nanostructure [16], size and nuclear distribution of transcription complexes [46,
3 47], replication factories [53] and repair complexes [45], nuclear pore complex distribution
4 [48], arrangement of polyribosomes. An additional important application will be the
5 possibility to count single molecules. Although the 2CLM technique allowed us to register
6 only a part of all labeled molecules, the figures obtained are minimum absolute numbers.
7 For example, a count of 90000 proteins in an optical section of a human fibroblast nucleus
8 of $10 \times 10 \mu\text{m} = 100 \mu\text{m}^2$ results in a molecule density of about $900/\mu\text{m}^2$. Even at the best
9 corresponding conventional optical resolution only a few thousand molecules would be
10 resolvable in a nuclear area of $100 \mu\text{m}^2$, corresponding to a density of resolved molecules
11 of about $30 \text{ molecules}/\mu\text{m}^2$. Since many protein types in the cells occur in numbers in the
12 order of 10^4 to 10^5 , 2CLM and related SALM methods for the first time promise to count
13 fluorescently labeled molecules in the cell even at such high numbers and densities.
14 Presently, the number of molecules counted is a relative number since it is not known to
15 what percentage the molecules can be excited in the way required for this type of
16 localization microscopy (which might be true also for other SALM methods). It is expected
17 that by appropriate calibration methods, even absolute numbers of individual molecules will
18 become countable, down to only a few molecules of a given type in an entire cell. If
19 conditions can be realized to induce fluorescence in a substantial part of such molecules
20 the sensitivity of this method might become superior even to techniques based on
21 radioactive decay: To reliably determine the number of a few radioactively labeled
22 molecules in a cell, one has to apply registration for at least several life times of the
23 radioactive substance used for labeling. For radioactive elements used in biology and
24 medicine, these times would be prohibitively long. In addition to an effective optical
25 resolution in the macromolecular range, this will open perspectives for many additional
26 applications on the single cell level, such as high precision monitoring of specific DNA
27 sequence amplification, gene expression, fast counting of virus particles inside and outside
28 cells at a spatial resolution equivalent to conventional electron microscopy, counting of
29 proteins in intracellular normal and pathological aggregates, or counting of drug molecules
30 present in specific nanoregions across the cell membrane.

31 5. ACKNOWLEDGEMENTS

32
33 The authors thank Prof. Markus Sauer (Bielefeld University), Dr. Michael Wassenegger (AIPlanta,
34 Neustadt/Weinstraße) and Dr. Victor Sourjik (ZMBH, University of Heidelberg) for support. We are grateful to
35 Patrick Varga-Weisz (Babraham Institute, Cambridge) for providing plasmid vectors. The financial support of
36 the State of Baden-Württemberg and of the Deutsche Forschungsgemeinschaft (SPP1128) to both Christoph
37 Cremer and Karsten Rippe (also grant Ri 1283/8-1) and of the European Union (In Vivo Molecular Imaging
38 Consortium, www.molimg.gr) is gratefully acknowledged. We also thank our colleagues Thibaud Jegou,
39 Thomas Ruckelshausen, David Baddeley, Jürgen Reymann, Alexander Brunner, Alexa von Bassewitz, Heinz
40 Eipel and Margund Bach for great support. Paul Lemmer is a Ph.D. student fellow of the Hartmut Hoffmann-
41 Berling International Graduate School of Molecular and Cellular Biology of the University of Heidelberg and a
42 member of the Excellence Cluster Cellular Networks of the University of Heidelberg; Rainer Kaufmann is a
43 Ph.D. student fellow in a Frontierproject of the Marsilius College University Heidelberg.
44
45
46
47
48
49
50
51
52
53
54
55
56
57
58
59
60

6. REFERENCES

- (1) Cremer, T., *Von der Zellenlehre zur Chromosomentheorie*, Springer-Verlag Berlin Heidelberg 1985. Download: http://humangenetik.bio.lmu.de/service/downloads/buch_tc/index.html.
- (2) Cremer, T., Cremer, C., Chromosome territories, nuclear architecture and gene regulation in mammalian cells. *Nature Reviews Genetics* 2001, 2, 292-301.
- (3) Abbe, E., Beiträge zur Theorie des Mikroskops und der mikroskopischen Wahrnehmung. *Archiv f. mikroskopische Anatomie* 1873, 9, 411-468.
- (4) Rayleigh, L., On the theory of optical images, with special reference to the microscope. *Philosophical Magazine* 1896, 42(5), 167-195.
- (5) Hell, S.W., Lindek, S., Cremer, C., Stelzer, E.H.K., Measurement of the 4Pi-confocal point spread function proves 75 nm axial resolution. *Applied Physics Letters* 1994, 64, 1335.
- (6) Hell, S.W., Toward fluorescence nanoscopy. *Nature Biotechnology* 2003, 2 (11), 1347-1355.
- (7) Heintzmann, R., Cremer, C., Lateral modulated excitation microscopy: Improvement of resolution by using a diffraction grating. *Proc. SPIE* 1999, 356, 185-196.
- (8) Gustafsson, M., Shao, L., Carlton, P.M., Wang, C.J.R. et al., Three-Dimensional Resolution Doubling in Wide-Field Fluorescence Microscopy by Structured Illumination. *Biophysical Journal* 2008, 94(12), 4957-4970.
- (9) Hell, S.W., Far-Field Optical Nanoscopy. *Science* 2007, 316(5828), 1153-1158.
- (10) Schmidt, R., Egner, A., Hell, SW, isoSTED Microscopy. *Frontiers in Optics* 2008.
- (11) Bornfleth, H., Sätzler, E.H.K, Eils, R., Cremer, C. High-precision distance measurements and volume-conserving segmentation of objects near and below the resolution limit in three-dimensional confocal fluorescence microscopy. *Journal of Microscopy* 1998, 189(2), 118–136.
- (12) Cremer, C. et al., German Patent Application No. 196.54.824.1/DE, submitted Dec 23, 1996, European Patent EP 1997953660, 08.04.1999, Japanese Patent JP 1998528237, 23.06.1999, United States Patent US 09331644, 25.08.1999
- (13) Heilemann, M., Herten, D.P., Heintzmann, R., Cremer, C. et al., High-resolution colocalization of single dye molecules by fluorescence lifetime imaging microscopy. *Analytical Chemistry* 2002, 74(14), 3511–3517.
- (14) Cremer, C., Edelmann, P., Bornfleth, H., Kreth, G. et al., Principles of Spectral Precision Distance confocal microscopy for the analysis of molecular nuclear structure, in: Jähne, B. (Ed.), Haußecker, H. (Ed.), Geißler, P. (Ed.), *Handbook of Computer Vision and Applications*, Academic Press, Inc. Orlando 1999, pp. 839-857.
- (15) Edelmann, P., Esa, A., Hausmann M., Cremer, C., Confocal laser scanning microscopy: In situ determination of the confocal point-spread function and the chromatic shifts in intact cell nuclei. *Optik* 1999, 110, 194-198.
- (16) Esa, A., Edelmann, P., Kreth, G., Trakhtenbrot, L. et al., Three-dimensional spectral precision distance microscopy of chromatin nanostructures after triple-colour DNA labelling: a study of the BCR region on chromosome 22 and the Philadelphia chromosome. *Journal of Microscopy* 2000, 199(2), 96–105.
- (17) Lacoste, T.D., Michalet, X., Pinaud, F., Chemla, D.S. et al., Ultrahigh-resolution multicolor colocalization of single fluorescent probes. 2000, 97(17), 9461-9466.

- 1
2 (18) Schmidt, M., Nagorni, M., Hell, S.W., Subresolution axial distance measurements in far-field
3 fluorescence microscopy with precision of 1 nanometer. *Review of Scientific Instruments* 2000, 71,
4 2742.
- 5 (19) Rauch J., Hausmann M., Solovei, I., Horsthemke B. et al., Measurement of local chromatin
6 compaction by Spectral Precision Distance microscopy. *Proc. SPIE* 2000, 4164, 1-9.
- 7 (20) Betzig, E., Patterson, G.H., Sougrat, R., Lindwasser, O.W. et al., Imaging Intracellular Fluorescent
8 Proteins at Nanometer Resolution. *Science* 2006, 313(5793), 1642–1645.
- 9 (21) Hess, S., Girirajan, T., Mason, M. Ultra-High Resolution Imaging by Fluorescence Photoactivation
10 Localization Microscopy. *Biophysical Journal* 2006, 91(11), 4258-4272.
- 11 (22) Rust, M., Bates, M., Zhuang, X., Sub-diffraction-limit imaging by stochastic optical reconstruction
12 microscopy (STORM). *Nature Methods* 2006, 3, 793-795.
- 13 (23) Egner, A., Geisler, C., von Middendorff, C., Bock, H. et al., Fluorescence nanoscopy in whole cells by
14 by asynchronous localization of photoswitching emitters. *Biophysical Journal* 2007, 93, 3285-3290.
- 15 (24) Andresen, M., Stiel, A.C., Jonas, F., Wenzel, D. et al., Photoswitchable fluorescent proteins enable
16 monochromatic multilabel imaging and dual color fluorescence nanoscopy. *Nature Biotechnology*
17 2008, 26 (9), 1035-1040.
- 18 (25) Reymann, J., Baddeley, D., Gunkel, M., Lemmer, P. et al., High-precision structural analysis of
19 subnuclear complexes in fixed and live cells via spatially modulated illumination (SMI) microscopy.
20 *Chromosome Research* 2008, 16(3), 367–382.
- 21 (26) Lemmer, P., Gunkel, M., Baddeley, D., Kaufmann, R. et al., SPDM: Light microscopy with single-
22 molecule resolution at the nanoscale. *Applied Physics B* 2008, 93(1), 1-12.
- 23 Lemmer P., C. Cremer, D. Baddeley, H. Eipel, Procedure and setup for localization of single
24 fluorophores in fluorescence microscopy, German Patent Application, submitted March 19, 2008.
- 25 (27) Heilemann M., van de Linde S., Schüttelpeiz M., Kasper R. et al., Subdiffraction-Resolution
26 Fluorescence Imaging with Conventional Fluorescent Probes. *Angew. Chemie* 2008, Int. Ed 47, 6172
27 -6176.
- 28 (28) R. Kaufmann, P. Lemmer, M. Gunkel, Y. Weiland et al., SPDM – Single Molecule Superresolution of
29 Cellular Nanostructures. *Proc. SPIE* 2009, 7185, 71850J.
- 30 (29) Burns, D.H., Callis, J.B., Christian, G.D., Davidson, E.R., Strategies for attaining superresolution
31 using spectroscopic data as constraints. *Applied Optics* 1985, 24 (2), 154-161.
- 32 (30) Betzig, E., Proposed method for molecular optical imaging. *Optics Letters* 1995, 20, 237.
- 33 (31) van Oijen, A.M., Köhler, J., Schmidt, J., Müller, M. et al., 3-Dimensional super-resolution by spectrally
34 selective imaging. *Chemical Physics Letters* 1998, 192(1-2), 182-187.
- 35 (32) Cremer, C., Failla, A., V., Albrecht, B., United States Patent No. US 7,298,461 B2 submitted Oct 9,
36 2001.
- 37 (33) Cremer, C., German Patent Application 2116521, (1971).
- 38 (34) Sinnecker, D., Voigt, P., Hellwig, N., Schaefer, M., Reversible photobleaching of enhanced green
39 fluorescent proteins. *Biochemistry* 2005, 44 (18), 7085-7094.
- 40 (35) Patterson, G.H., Lippincott-Schwartz, J., A Photoactivatable GFP for Selective Photolabeling of
41 Proteins and Cells. *Science* 2002, 297 (5588), 1873-1877.
- 42 (36) Hendrix, J., Flors, C., Dedecker, P., Hofkens, J. et al., Dark States in Monomeric Red Fluorescent
43 Proteins Studied by Fluorescence Correlation and Single Molecule Spectroscopy. *Biophysical Journal*
44 2008, 94 (10), 4103.
- 45
46
47
48
49
50
51
52
53
54
55
56
57
58
59
60

- 1
2 (37) Baddeley D., Jayasinghe I.D., Cremer C., Cannell M.B. et al., Light-induced dark states of organic
3 fluorochromes enable 30 nm resolution imaging in standard media. *Biophysical J.*, in press.
- 4 (38) van Holde, K.E. *Chromatin*, Springer, Heidelberg 1989.
- 5 (39) Becker, P.B., Horz, W., ATP-dependent nucleosome remodeling. *Annu Rev Biochem* 2002, 71, 247-
6 273.
- 7 (40) Cairns, B.R., Chromatin remodeling: insights and intrigue from single-molecule studies. *Nat Struct*
8 *Mol Biol* 2007, 14, 989-996.
- 9 (41) Rippe, K., Schrader, A., Riede, P., Strohner, R., et al., DNA sequence- and conformation-directed
10 positioning of nucleosomes by chromatin-remodeling complexes. *Proc. Natl. Acad. Sci. USA* 2007,
11 104, 15635-15640.
- 12 (42) Langst, G., Becker, P.B., Nucleosome mobilization and positioning by ISWI-containing chromatin-
13 remodeling factors. *J. Cell Sci.* 2001, 114, 2561-2568.
- 14 (43) Collins, N., Poot, R.A., Kukimoto, I., Garcia-Jimenez, C. et al., An ACF1-ISWI chromatin-remodeling
15 complex is required for DNA replication through heterochromatin. *Nat. Genet.* 2002,32, 627-632.
- 16 (44) Lemmer P., Gunkel M., Baddeley D., Kaufman R. et al., Using conventional fluorescent markers for
17 far-field fluorescence nanoscopy allows resolution in the 10 nm range. revised version submitted.
- 18 (45) Hauptner, A., Krucken, R., Greubel, C., Hable, V. et al., DNA-repair protein distribution along the
19 tracks of energetic ions. *Radiation protection dosimetry* 2006, 122, 147-149.
- 20 (46) Rauch J., Knoch T.A., Solovei I., Teller K. et al., Lightoptical precision measurements of the active
21 and inactive Prader-Willi Syndrome imprinted regions in human cell nuclei. *Differentiation* 2008, 76:
22 66-83.
- 23 (47) Martin S., Failla A.V., Spoeri U., Cremer C. et al., Measuring the Size of Biological Nanostructures
24 with Spatially Modulated Illumination Microscopy. *Molecular Biology of the Cell* 2004, 15: 2449–2455.
- 25 (48) Schermelleh, L., Carlton, P.M., Haase, S., Shao, L. et al., Subdiffraction multicolor imaging of the
26 nuclear periphery with 3d structured illumination microscopy, *Science* 2006, 320, 1332-1336.
- 27 (49) Fölling, J., Bossi, M., Bock, H., Medda, R. et al., Fluorescence nanoscopy by ground-state depletion
28 and single-molecule return. *Nature Methods* 2008, 5(11), 943-945.
- 29 (50) S. van de Linde, M Sauer, M Heilemann, Subdiffraction-resolution fluorescence imaging of proteins in
30 the mitochondrial inner membrane with photoswitchable fluorophores. *Journal of Structural Biology*
31 *2008*, 164, 250-254.
- 32 (51) S. van de Linde, R Kasper, M Heilemann, M Sauer, Photoswitching microscopy with standard
33 fluorophores. *Applied Physics B* 2008, 93, 725-731.
- 34 (52) Rittweger, E., Han, K.Y., Irvine, S.E., Eggeling, C. et al., STED microscopy reveals crystal colour
35 centres with nanometric resolution. *Nature Photonics* 2009, 3, 144-147.
- 36 (53) Leonhardt, H., Rahn, H.P., Weinzierl, P., Sporbert, A. et al., Dynamics of DNA replication factories in
37 living cells, *Journal of Cell Biology* 2000,149, 271-280.
- 38
39
40
41
42
43
44
45
46
47
48
49
50
51
52
53
54
55
56
57
58
59
60

Figure Legends:

Figure 1. Microscope setup. Schematic representation of the microscopic setup for 2 CLM.
DM1, DM2: dichroic elements, L1 – L4: lenses or lens systems, BF1 (interchangeable

1
2 blocking filter): dichroic elements to block the illumination light (488 nm, 568 nm). GFP
3 fluorescence emission (emission maximum @ $\lambda_{em} = 520$ nm) is transmitted through a
4 bandpass filter (HQ 525/50), mRFP1 fluorescence emission (emission maximum @ $\lambda_{em} =$
5 584 nm) is transmitted through a triple line blocking filter (488/568/647nm). From Lemmer
6 et al. 2009 [44].
7
8

9 **Figure 2.** Simulation of 2CLM. First row: Dual color object in three different label densities
10 (left: 50000 molecules/ μm^2 , middle: 5000 molecules/ μm^2 , right: 500 molecules/ μm^2) is
11 imaged using different assumptions. Second row: Conventional epifluorescence
12 microscopy with NA 1.4, 100 nm pixel size, 520 nm/580 nm emission wavelength. The size
13 of the scalebar is 500 nm. Third row: 2CLM image with 20 nm mean localization accuracy.
14 Last row: 2CLM image with 10 nm mean localization accuracy. The single molecule
15 positions in the 2CLM images are blurred with a Gaussian kernel corresponding to the
16 estimated mean localization accuracy of the process.
17

18 **Figure 3.** Distribution of H2A proteins within a human U2OS nucleus. (A) Conventional
19 epifluorescence image. (B) 2CLM image, each mRFP1-position is blurred with a Gaussian
20 representing the individual localization accuracy. Panel C and D display enlarged regions.
21 Scale bars are 2 μm in A and B and 500 nm in C and D.
22

23 **Figure 4.** Distribution of Snf2H proteins within a human U2OS nucleus. (A) Conventional
24 epifluorescence image. (B) 2CLM image, each GFP-position is blurred with a Gaussian
25 representing the individual localization accuracy. Panel C and D display enlarged regions.
26 Scale bars are 2 μm in A and B and 500 nm in C and D.
27

28 **Figure 5.** Distribution of H2A proteins (red) and Snf2H proteins (green) within a human
29 U2OS nucleus. (A) Conventional epifluorescence image. (B) 2CLM image, each
30 fluorochrome-position is blurred with a Gaussian representing the individual localization
31 accuracy. Panel C and D display enlarged regions. Scale bars are 2 μm in A and B and
32 500 nm in C and D.
33

34 **Figure 6.** Localization accuracy. (A) Histogram of localization accuracies of GFP and
35 mRFP1 for one cell determined by the fitting algorithm. The lower accuracy for mRFP1 (38
36 ± 4 nm) was due to a lower number of photon counts (see supplementary material). (B)
37 Comparison of conventional epifluorescence and 2CLM image. In the latter one, two
38 molecule positions with a distance of about 30 nm can be resolved (both recorded within 7
39 s, corresponding to an estimated drift of about 1 nm). The pixel size in the epifluorescence
40 image is 65 nm.
41
42
43
44
45
46
47
48
49
50
51
52
53
54
55
56
57
58
59
60

1
2 **Figure 7.** Visualization of particle densities. A histogram of the number of neighbors (of the
3 same color) within a circle of 300 nm radius was plotted for H2A (A) and Snf2H (B) for the
4 cell below. As a reference, the same histograms were plotted for random distributions with
5 equal particle densities. Experimentally observed histograms were broader than the
6 histograms for random distributions and could only be fitted considering different particle
7 populations. Based on these histograms, density maps for H2A (C) and Snf2H (D) were
8 derived to separate particles in the low-density population (blue/red), the high-density
9 population (green) and the densest 10 % (yellow). Arrows in panel C highlight regions of
10 colocalization between H2A and Snf2H, arrows in panel D highlight regions of anti-
11 colocalization.
12

13
14 **Figure 8.** Colocalization analysis of H2A and Snf2H. For H2A (A) and Snf2H (D) in a typical
15 cell a histogram of the distance to the nearest neighbor in the other color was plotted.
16 Based on the average distances, two length-scales were chosen for which the number of
17 different colored neighbors was shown in a histogram (B, C, E, F). As a reference, the
18 number of neighbors in a random distribution with corresponding densities is shown.
19 Experimentally observed histograms were broader than the histograms for random
20 distributions, reflecting the heterogeneity of the density. Furthermore, the average number
21 of neighbors is larger than for a random distribution, suggesting partial colocalization
22 between H2A and Snf2H.
23
24
25
26
27
28
29
30
31
32
33
34
35
36
37
38
39
40
41
42
43
44
45
46
47
48
49
50
51
52
53
54
55
56
57
58
59
60

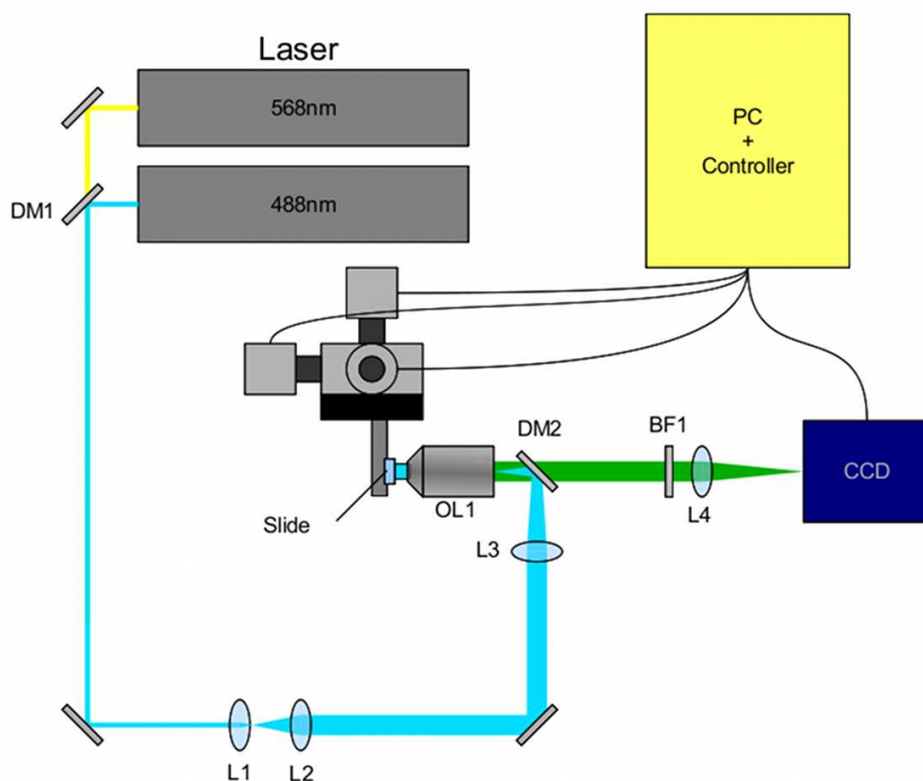


Figure 1: Microscope setup. Schematic representation of the microscopic setup for 2 CLM. DM1, DM2: dichroic elements, L1 – L4: lenses or lens systems, BF1 (interchangeable blocking filter): dichroic elements to block the illumination light (488 nm, 568 nm). GFP fluorescence emission (emission maximum @ $\lambda_{em} = 520$ nm) is transmitted through a bandpass filter (HQ 525/50), mRFP1 fluorescence emission (emission maximum @ $\lambda_{em} = 584$ nm) is transmitted through a triple line blocking filter (488/568/647nm). From Lemmer et al. 2009 [44].
99x84mm (300 x 300 DPI)

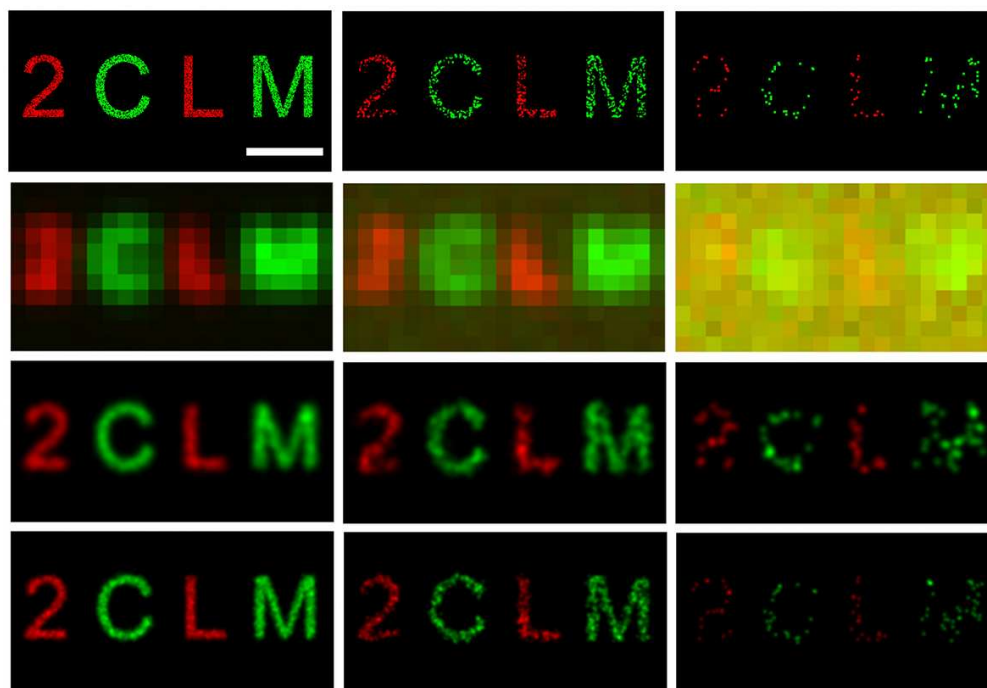


Figure 2: Simulation of 2CLM. First row: Dual color object in three different label densities (left: 50000 molecules/ μm^2 , middle: 5000 molecules/ μm^2 , right: 500 molecules/ μm^2) is imaged using different assumptions. Second row: Conventional epifluorescence microscopy with NA 1.4, 100 nm pixel size, 520 nm/580 nm emission wavelength. The size of the scalebar is 500 nm. Third row: 2CLM image with 20 nm mean localization accuracy. Last row: 2CLM image with 10 nm mean localization accuracy. The single molecule positions in the 2CLM images are blurred with a Gaussian kernel corresponding to the estimated mean localization accuracy of the process.
99x69mm (300 x 300 DPI)

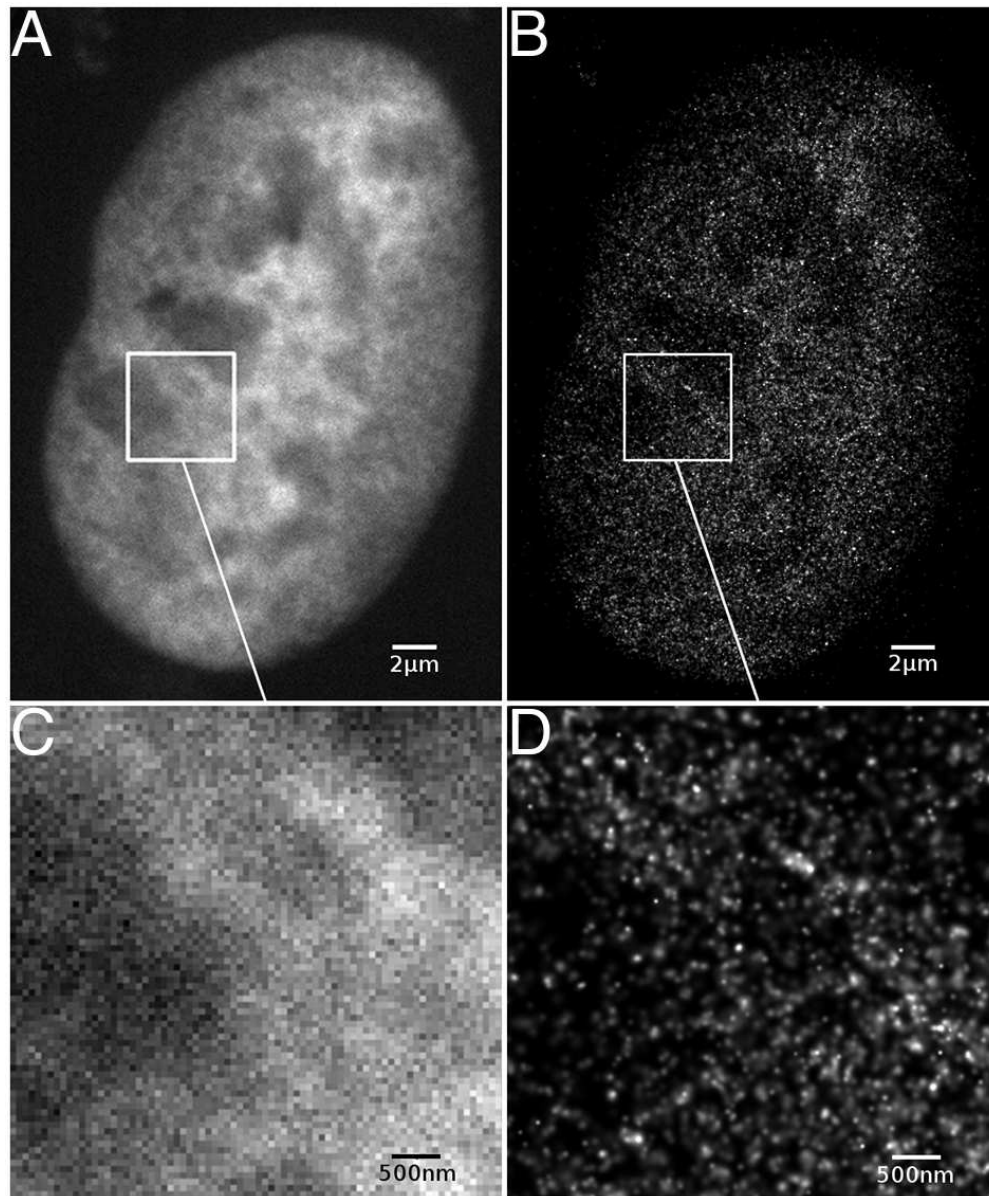


Figure 3: Distribution of H2A proteins within a human U2OS nucleus. (A) Conventional epifluorescence image. (B) 2CLM image, each mRFP1-position is blurred with a Gaussian representing the individual localization accuracy. Panel C and D display enlarged regions. Scale bars are 2 μm in A and B and 500 nm in C and D.
80x96mm (300 x 300 DPI)

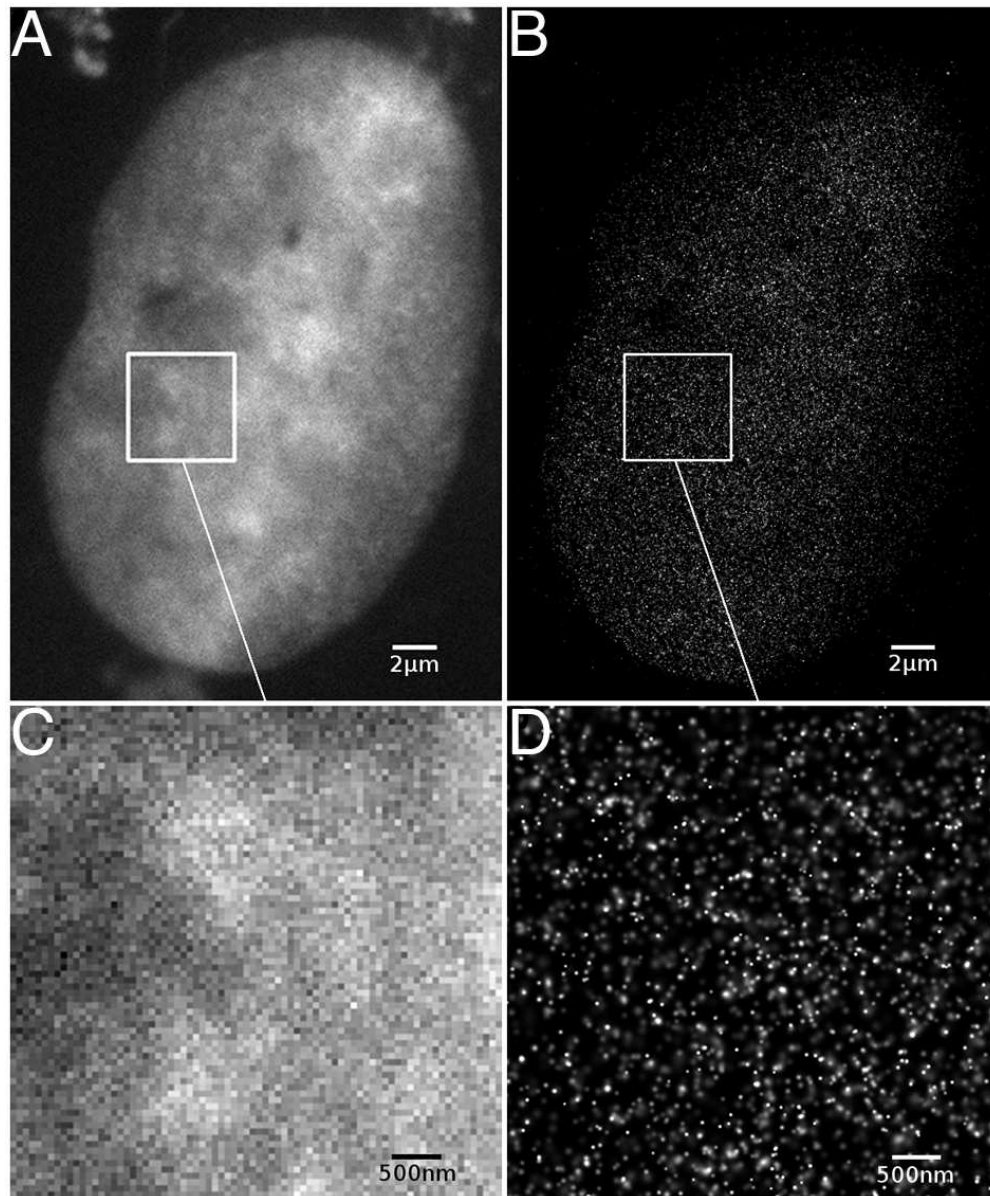


Figure 4: Distribution of Snf2H proteins within a human U2OS nucleus. (A) Conventional epifluorescence image. (B) 2CLM image, each GFP-position is blurred with a Gaussian representing the individual localization accuracy. Panel C and D display enlarged regions. Scale bars are 2 μm in A and B and 500 nm in C and D.
80x96mm (300 x 300 DPI)

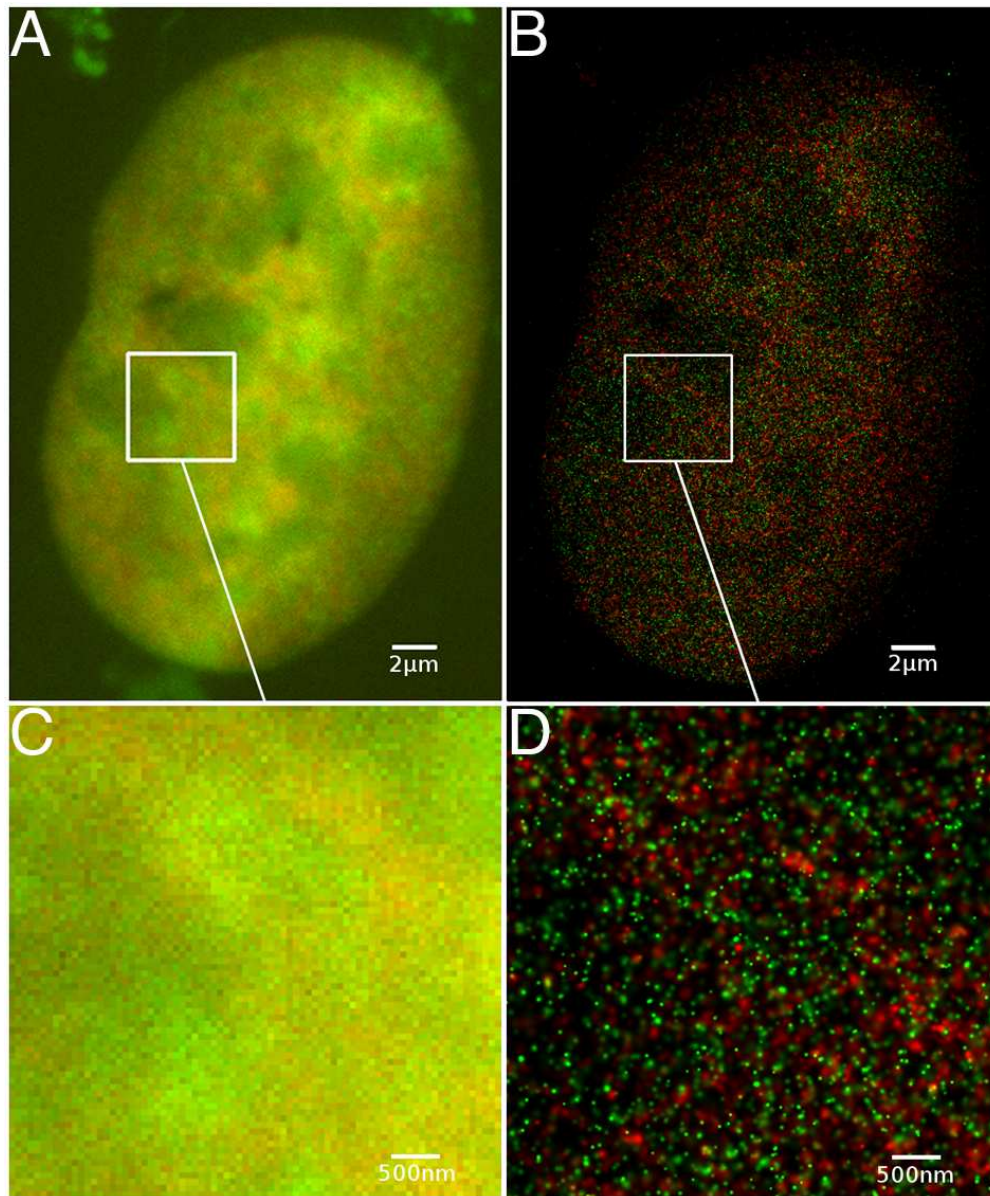


Figure 5: Distribution of H2A proteins (red) and Snf2H proteins (green) within a human U2OS nucleus. (A) Conventional epifluorescence image. (B) 2CLM image, each fluorochrome-position is blurred with a Gaussian representing the individual localization accuracy. Panel C and D display enlarged regions. Scale bars are 2 μm in A and B and 500 nm in C and D.
80x96mm (300 x 300 DPI)

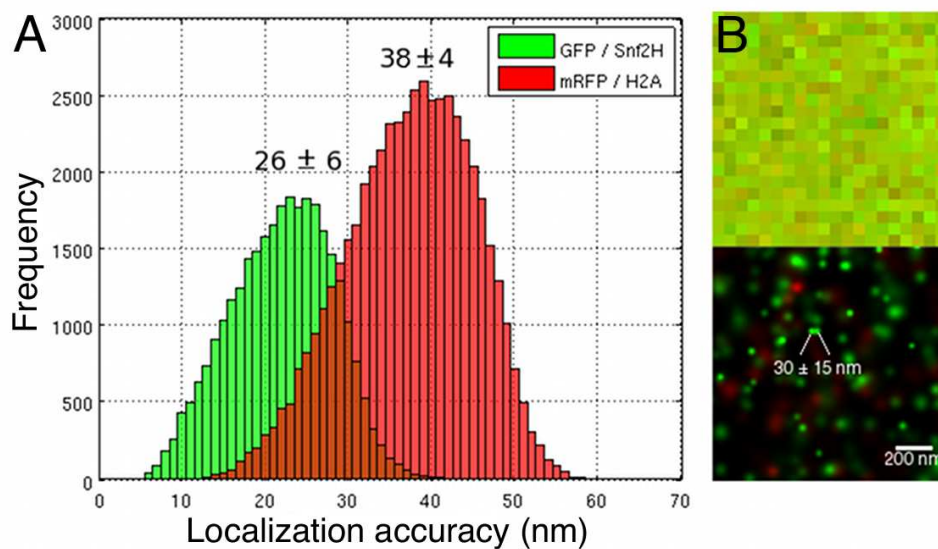


Figure 6: Localization accuracy. (A) Histogram of localization accuracies of GFP and mRFP1 for one cell determined by the fitting algorithm. The lower accuracy for mRFP1 (38 ± 4 nm) was due to a lower number of photon counts (see supplementary material). (B) Comparison of conventional epifluorescence and 2CLM image. In the latter one, two molecule positions with a distance of about 30 nm can be resolved (both recorded within 7 s, corresponding to an estimated drift of about 1 nm). The pixel size in the epifluorescence image is 65 nm.
99x55mm (300 x 300 DPI)

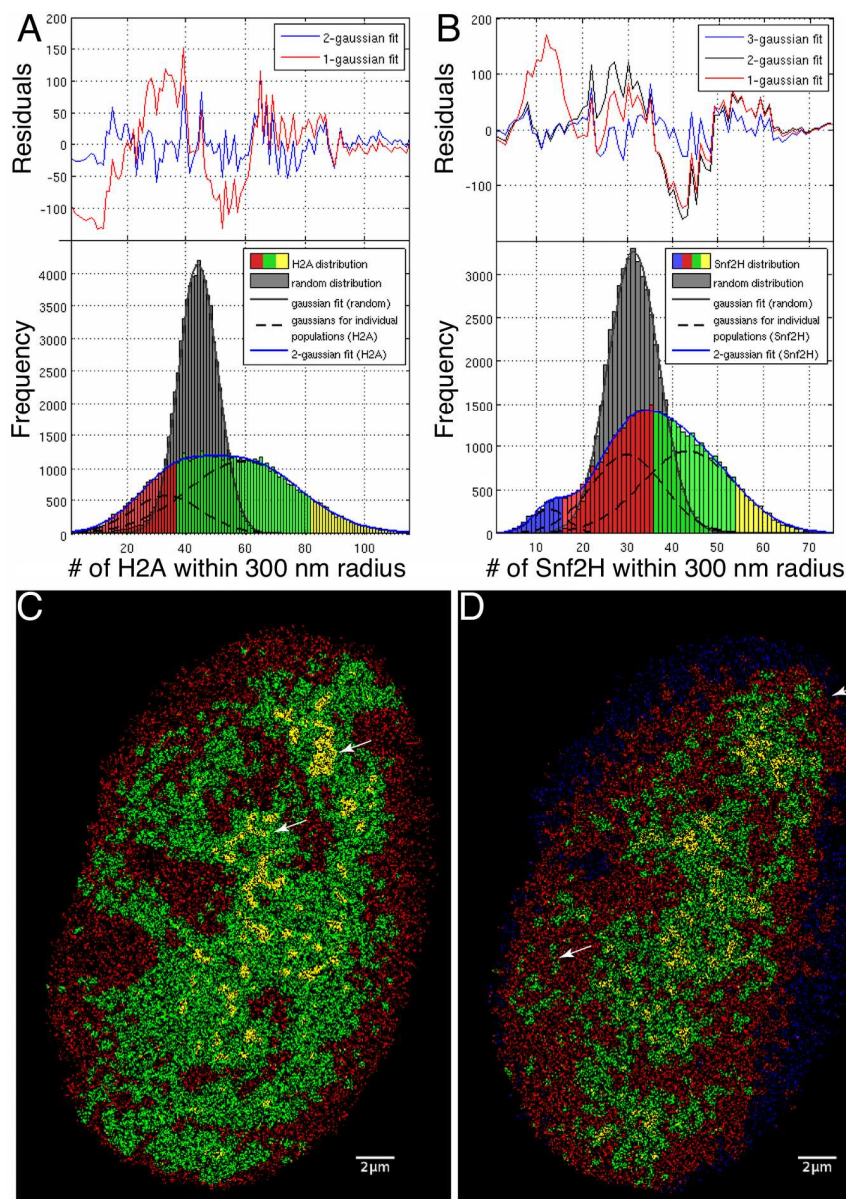


Figure 7: Visualization of particle densities. A histogram of the number of neighbors (of the same color) within a circle of 300 nm radius was plotted for H2A (A) and Snf2H (B) for the cell below. As a reference, the same histograms were plotted for random distributions with equal particle densities. Experimentally observed histograms were broader than the histograms for random distributions and could only be fitted considering different particle populations. Based on these histograms, density maps for H2A (C) and Snf2H (D) were derived to separate particles in the low-density population (blue/red), the high-density population (green) and the densest 10 % (yellow). Arrows in panel C highlight regions of colocalization between H2A and Snf2H, arrows in panel D highlight regions of anti-colocalization.

119x160mm (300 x 300 DPI)

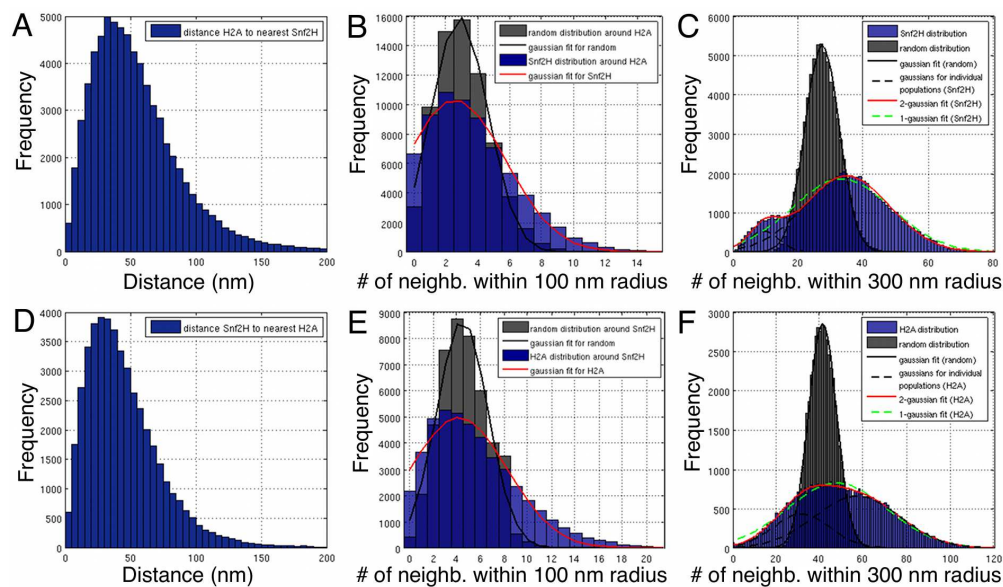


Figure 8: Colocalization analysis of H2A and Snf2H. For H2A (A) and Snf2H (D) in a typical cell a histogram of the distance to the nearest neighbor in the other color was plotted. Based on the average distances, two length-scales were chosen for which the number of different colored neighbors was shown in a histogram (B, C, E, F). As a reference, the number of neighbors in a random distribution with corresponding densities is shown. Experimentally observed histograms were broader than the histograms for random distributions, reflecting the heterogeneity of the density. Furthermore, the average number of neighbors is larger than for a random distribution, suggesting partial colocalization between H2A and Snf2H.

160x93mm (300 x 300 DPI)